Equivalent Impedance Parameter Calculation of Three-phase Symmetrical Loads for Harmonic Source Location

Yi Zhang, Bijie Liu, Caihua Lin, Zhenguo Shao, and Yuncong Xu

***Abstract*—The equivalent impedance parameters of loads have been widely used to identify and locate the harmonic sources. However, the existing calculation methods suffer from outliers caused by the zero-crossing of the denominator. These outliers can result in inaccuracy and unreliability of harmonic source location. To address this issue, this paper proposes an innovative method of equivalent impedance parameter calculation of three-phase symmetrical loads that avoid outliers. The correctness and effectiveness of the proposed method are verified by simulations on Simulink using actual monitoring data. The results show that the proposed method is not only simple and easy to implement but also highly accurate.**

***Index Terms*—abc-$\alpha\beta$ transformation, equivalent impedance parameters of load, harmonic source location, nonlinear load, power quality.**

I. Introduction

WITH a large number of distributed generations and nonlinear loads in power grids, harmonic distortion has become one of the most common and significant power-quality-related problems, which has attracted increasing research attention in recent years [1], [2]. Harmonic sources in power grids must be identified and located to achieve effective control of harmonic pollution and determination of responsibility in incentive management [3]-[5].

Nonlinear loads are considered as harmonic sources since they can actively emit harmonic currents to the power grid, which contribute to the harmonic voltage at the point of common coupling (PCC). However, linear loads cannot actively emit a harmonic current but can produce a harmonic current in the presence of background harmonic voltages. Therefore, harmonic magnitude measurement of load currents cannot be used directly for harmonic source location [6].

Researchers have long been dedicated to developing efficient harmonic source location methods to lay a foundation for harmonic responsibility division and harmonic mitigation. The existing harmonic source location methods can be roughly divided into two categories: methods based on an equivalent circuit model, and methods based on harmonic state estimation.

The former methods divide an equivalent circuit model into two sides, i.e., the system side and the user side at the PCC, and locate the harmonic source using various positioning techniques such as active or reactive harmonic power direction and harmonic impedance information [7]-[10]. The operational principle of this type of method is simple and intuitive, but these methods can locate the harmonic source for only one node at a time. Therefore, they are generally applied to single-harmonic source systems. Unfortunately, it has been demonstrated that the power-direction methods can provide incorrect results in certain situations, which makes them unreliable for identifying harmonic sources [11], [12]. In addition, the harmonic impedance calculation methods are vulnerable to background harmonic fluctuation and affected by harmonic impedance correlation [13].

The harmonic source location methods based on harmonic state estimation can determine the distribution of harmonic voltage and harmonic current of the whole system, allowing it to trace multiple harmonic sources throughout the system [14]-[17]. Therefore, these methods have gradually become the focus of current research. The main step in these methods is to obtain the measurement data on the power grid using an acquisition system, establish the parameter matrix based on the network topology and component harmonic parameters, solve the harmonic state estimation equation, and identify the harmonic source by injecting active power at harmonic frequencies. However, modern distribution networks show obvious dynamic characteristics. The network parameters and topology frequently change at a non-fundamental frequency, which is often difficult to obtain accurately, making this type of method difficult to apply in practical engineering.

As the time-varying equivalent impedance parameters of the load are the primary cause of harmonic generation in nonlinear loads, a harmonic source location method based on parameter identification has been proposed in [18]-[20]. This method can analyze the voltage and current waveforms

Manuscript received: August 4, 2022; revised: November 6, 2022; accepted: April 24, 2023. Date of CrossCheck: April 24, 2023. Date of online publication: August 8, 2023.

This work was supported by the National Natural Science Foundation of China (No. 51777035).

Y. Zhang, B. Liu, Z. Shao, and Y. Xu are with the Department of Electrical Engineering and Automation, Fuzhou University, Fuzhou, China (e-mail: zhangyi@fzu.edu.cn; fzu-ee-liu@foxmail.com; shao.zg@fzu.edu.cn; 1360397798@qq.com).

C. Lin (corresponding author) is with State Grid Fujian Electric Power Research Institute, Fuzhou, China (e-mail: lin.ch@foxmail.com).

DOI: 10.35833/MPCE.2022.000492

at the PCC to solve equivalent impedance parameters of different loads. The parameter identification method can be used in most cases because the voltage and current waveforms are sufficient for harmonic source location [21], [22]. Abnormal fluctuations and glitches can be frequently observed in time-domain equivalent parameter waveforms and are often considered as outliers in numerical results. These outliers could result in inaccuracy and unreliability of harmonic source location. Numerical precision-enhancing methods such as the singular value decomposition (SVD) method can be used in parameter-solving processes, but they are not very effective in improving the results [21]. Although the outlier phenomenon in harmonic source location based on the parameter identification method has been investigated and validated [21], and the applicability of this method has been discussed, the outlier problem has not been solved yet.

The purpose of this paper is to improve the calculation method of equivalent impedance parameters of three-phase symmetrical loads to reduce the influence of outliers on the harmonic source location.

The main contributions of this paper can be summarized as follows.

1) A new method for equivalent impedance parameter calculation of three-phase symmetrical loads is proposed to avoid the problem of outliers.

2) The proposed method is applied to the analysis of nonlinear loads, and its advantages over the existing methods in the field of harmonic source location are verified.

The rest of this paper is organized as follows. Section II introduces the basic principles of the parameter identification method for harmonic source location and formulates the outlier problem. Section III presents a novel equivalent impedance calculation method of three-phase symmetrical loads. Section IV presents case study that validates the proposed method by simulations using actual monitoring data. Finally, Section V concludes this paper and presents future work.

II. Basic Principles

Two types of equivalent load models, i.e., a parallel impedance model and a series impedance model, have been commonly used in harmonic source location based on a parameter identification method. As shown in Fig. 1, considering that the majority of nonlinear loads in power systems are inductive and resistive, a series resistance-inductance impedance model that has been widely used in harmonic analysis is used as a research objective in this paper [18]-[22]. In Fig. 1, u, i, R, and L are the voltage, current, resistance, and reactance, respectively.

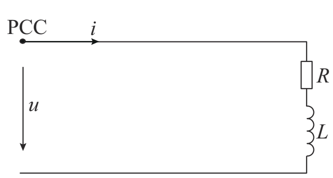

Fig. 1. Equivalent series impedance model in time domain.

In the series impedance model, it holds that:

$$u = iR + L\frac{\mathrm{d}i}{\mathrm{d}t} \tag{1}$$

Equations can be established by two adjacent sample data points using voltage and current signal sequences to determine the equivalent impedance parameters. Equations in the series impedance model can be established as follows:

$$\begin{bmatrix} u_1 \\ u_2 \end{bmatrix} = \begin{bmatrix} i_1 & i_1' \\ i_2 & i_2' \end{bmatrix} \begin{bmatrix} R \\ L \end{bmatrix} \tag{2}$$

where $u_1, u_2, i_1, i_2, i_1', i_2'$ are the adjacent sample point values in the corresponding signal sequences, and $i_k' = \mathrm{d}i_k/\mathrm{d}t$ $(k=1,2)$.

For obtaining a harmonic source location, the emitted harmonic magnitude can be used to determine harmonic sources using active models such as the Norton model at harmonic frequencies [23], as a traditional method in the frequency domain; also, the time-varying equivalent impedance parameters can be used to determine harmonic sources, as a method in the time domain. The equivalent impedance waveforms in the time domain are obtained by sequentially solving (2). In fundamental cycles of grid frequency, equivalent impedance waveforms of linear loads generally remain stable, while severe fluctuations in equivalent impedance waveforms of nonlinear loads are easily observed [6], [18]-[21].

Nonlinear loads are considered harmonic sources in power grids and can be identified by the non-linearity index (NLI) [20] using the equivalent impedance parameters.

The solution to (2) is given by:

$$\begin{bmatrix} R \\ L \end{bmatrix} = \begin{bmatrix} \dfrac{u_1 i_2' - u_2 i_1'}{i_1 i_2' - i_2 i_1'} \\[2ex] \dfrac{i_1 u_2 - i_2 u_1}{i_1 i_2' - i_2 i_1'} \end{bmatrix} \tag{3}$$

When the denominators in (3) cross zero, outliers will occur in equivalent impedance waveforms. Reference [21] has elaborated on the non-zero-crossing condition of denominators in (3), which can be expressed as (4a) or (4b).

$$\frac{I_h}{I_1} < \frac{1}{h^2} \tag{4a}$$

$$\frac{I_h}{I_1} > 1 \tag{4b}$$

where h is the order of harmonic current; I_h is the h^{th} harmonic current; and I_1 is the 1^{st} harmonic current. When the non-zero-crossing conditions are not satisfied, the denominators will cross zero and induce outliers. The outliers in equivalent impedance waveforms appear as isolated burrs with extremely large absolute values, as shown in Fig. 2.

In addition, in [21], it has been verified that the zero-crossing condition of denominators rather than numerical error is the major cause of the outlier problem, and thus, it is not appropriate to apply numerical precision enhancing methods such as the SVD method or outlier rejecting methods.

III. Novel Equivalent Impedance Calculation Method

In the actual operation of a power grid, the main causes of harmonic pollution are high-capacity three-phase loads in industrial production and new centralized energy power plants.

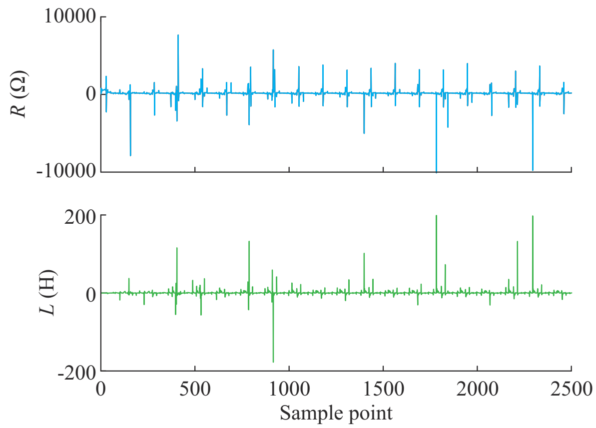

Fig. 2. Outliers in equivalent impedance waveforms.

Such loads are usually connected to the grid via three-phase wiring at the voltage level of 10 kV or above, and most of them are equipped with power quality monitoring devices. Therefore, (1) can be re-written as:

$$\begin{bmatrix} u_A \\ u_B \\ u_C \end{bmatrix} = \begin{bmatrix} i_A R_A + L_A \dfrac{\mathrm{d}i_A}{\mathrm{d}t} \\ i_B R_B + L_B \dfrac{\mathrm{d}i_B}{\mathrm{d}t} \\ i_C R_C + L_C \dfrac{\mathrm{d}i_C}{\mathrm{d}t} \end{bmatrix} \tag{5}$$

where u_A, u_B, u_C and i_A, i_B, i_C are the sample point values of three-phase voltage and current, respectively; and R_A, R_B, R_C and L_A, L_B, L_C are the resistance and inductance of a three-phase load, respectively.

Assuming a three-phase symmetrical load, namely $R_A = R_B = R_C = R$ and $L_A = L_B = L_C = L$, (5) can be re-written as follows:

$$\begin{bmatrix} u_A \\ u_B \\ u_C \end{bmatrix} = \begin{bmatrix} i_A & \dfrac{\mathrm{d}i_A}{\mathrm{d}t} \\ i_B & \dfrac{\mathrm{d}i_B}{\mathrm{d}t} \\ i_C & \dfrac{\mathrm{d}i_C}{\mathrm{d}t} \end{bmatrix} \begin{bmatrix} R \\ L \end{bmatrix} \tag{6}$$

Using the fast Fourier transformation (FFT), the current is decomposed into the sum of harmonic currents, which can be expressed by:

$$i_A = i_{A1} + i_{A2} + \ldots + i_{A3} = \sum_{h=1}^{H} i_{Ah} \tag{7}$$

where i_{Ah} is the instantaneous value of the h^{th} harmonic current.

Combining (6) and (7) yields:

$$\begin{bmatrix} i_A & \dfrac{\mathrm{d}i_A}{\mathrm{d}t} \\ i_B & \dfrac{\mathrm{d}i_B}{\mathrm{d}t} \\ i_C & \dfrac{\mathrm{d}i_C}{\mathrm{d}t} \end{bmatrix} = \sum_{h=1}^{H} \begin{bmatrix} i_{Ah} & \dfrac{\mathrm{d}i_{Ah}}{\mathrm{d}t} \\ i_{Bh} & \dfrac{\mathrm{d}i_{Bh}}{\mathrm{d}t} \\ i_{Ch} & \dfrac{\mathrm{d}i_{Ch}}{\mathrm{d}t} \end{bmatrix} \tag{8}$$

Then abc-$\alpha\beta$ transformation is adopted to three-phase voltage and current in (6), which can be written as follows:

$$\begin{bmatrix} u_\alpha \\ u_\beta \end{bmatrix} = \left(\sum_{h=1}^{H} \begin{bmatrix} i_{\alpha h} & \dfrac{\mathrm{d}i_{\alpha h}}{\mathrm{d}t} \\ i_{\beta h} & \dfrac{\mathrm{d}i_{\beta h}}{\mathrm{d}t} \end{bmatrix} \right) \begin{bmatrix} R \\ L \end{bmatrix} \tag{9}$$

Further, R and L can be solved by (9), but this process involves derivatives, which makes it complex for practical applications, so it needs to be simplified. The equations of instantaneous three-phase current are given by [24]:

$$\begin{cases} i_A = \displaystyle\sum_{h\in 3k+1} A_{1h}\cos\left(hwt + \varPhi_{1h}\right) + \sum_{h\in 3k+2} A_{2h}\cos\left(hwt + \varPhi_{2h}\right) + \\ \quad \displaystyle\sum_{h\in 3k+3} A_{0h}\cos\left(hwt + \varPhi_{0h}\right) \\ i_B = \displaystyle\sum_{h\in 3k+1} B_{1h}\cos\left(hwt + \varPhi_{1h} - \frac{2\pi}{3}\right) + \\ \quad \displaystyle\sum_{h\in 3k+2} B_{2h}\cos\left(hwt + \varPhi_{2h} + \frac{2\pi}{3}\right) + \sum_{h\in 3k+3} B_{0h}\cos\left(hwt + \varPhi_{0h}\right) \\ i_C = \displaystyle\sum_{h\in 3k+1} C_{1h}\cos\left(hwt + \varPhi_{1h} + \frac{2\pi}{3}\right) + \\ \quad \displaystyle\sum_{h\in 3k+2} C_{2h}\cos\left(hwt + \varPhi_{2h} - \frac{2\pi}{3}\right) + \sum_{h\in 3k+3} C_{0h}\cos\left(hwt + \varPhi_{0h}\right) \end{cases} \tag{10}$$

where $k \in \mathbf{N}$; A_{ih} B_{ih}, and C_{ih} $(i = 0, 1, 2)$ are the peak amplitudes of the h^{th} harmonic current of phases A, B, and C, respectively; $\varPhi_{ih}$ $(i = 0, 1, 2)$ is the initial phase angle of the h^{th} harmonic current; w is 314 rad/s or 377 rad/s at a basic frequency of 50 Hz or 60 Hz, respectively; and the subscripts "1", "2", and "0" represent positive-, negative-, and zero-sequence components, respectively.

Considering the three-phase symmetry, for the h^{th} positive-sequence and zero-sequence harmonic currents after the FFT, the phasor diagram is shown in Fig. 3, where i_{ah}, i_{bh}, and i_{ch} are phasors of the h^{th} harmonic current of phases A, B, and C, respectively.

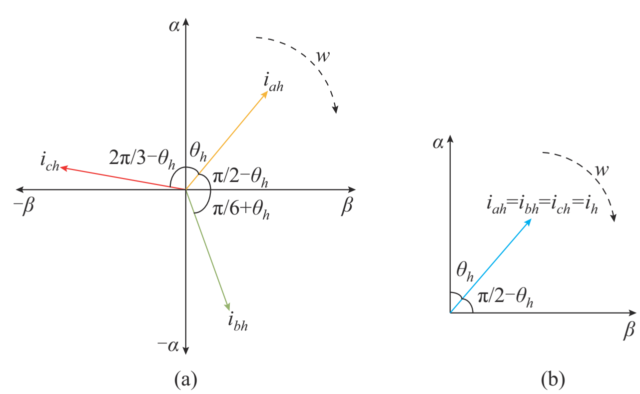

Fig. 3. Phasor diagram of the h^{th} positive-sequence and zero-sequence harmonic currents. (a) Positive-sequence harmonic current. (b) Zero-sequence harmonic current.

For the convenience of analysis, the initial phase angle $\varPhi_{ih}$ in (10) is assumed to be zero. Next, two cases presented in Fig. 3 are analyzed as follows:

A. Positive-sequence Harmonic Current

For the sequence presented in Fig. 3(a), the abc-$\alpha\beta$ transformation is adopted to the h^{th} positive-sequence harmonic current to obtain (11) and (12). The derivatives of $i_{\alpha h}$ and $i_{\beta h}$ are given by (13) and (14), respectively. For the h^{th} negative-sequence harmonic current, the similar equations can be obtained in the same way, but this paper does not provide unnecessary details on this topic.

$$i_{\alpha h}=A_h\cos\left(hwt+\theta_h\right)-B_h\cos\left(\frac{\pi}{3}-hwt-\theta_h\right)+ C_h\cos\left(\frac{2\pi}{3}-hwt-\theta_h\right) \tag{11}$$

$$i_{\beta h}=A_h\cos\left(\frac{\pi}{2}-hwt-\theta_h\right)+B_h\cos\left(\frac{\pi}{6}+hwt+\theta_h\right)- C_h\cos\left(-\frac{\pi}{6}+hwt+\theta_h\right) \tag{12}$$

$$\begin{aligned}\frac{\mathrm{d}i_{\alpha h}}{\mathrm{d}t}=&-hwA_h\sin\left(hwt+\theta_h\right)- hwB_h\left(\frac{-\sin\left(hwt+\theta_h\right)}{2}+\frac{\sqrt{3}\cos\left(hwt+\theta_h\right)}{2}\right)+\\ &hwC_h\left(\frac{\sin\left(hwt+\theta_h\right)}{2}+\frac{\sqrt{3}\cos\left(hwt+\theta_h\right)}{2}\right)=\\ &-hw\left(A_h\cos\left(\frac{\pi}{2}-hwt-\theta_h\right)+B_h\cos\left(\frac{\pi}{6}+hwt+\theta_h\right)-C_h\cos\left(-\frac{\pi}{6}+hwt+\theta_h\right)\right)=-hwi_{\beta h}\end{aligned} \tag{13}$$

$$\begin{aligned}\frac{\mathrm{d}i_{\beta h}}{\mathrm{d}t}=&-hwA_h\cos\left(hwt+\theta_h\right)+ hwB_h\left(\frac{-\sqrt{3}\sin\left(hwt+\theta_h\right)}{2}-\frac{\cos\left(hwt+\theta_h\right)}{2}\right)-\\ &hwC_h\left(\frac{-\sqrt{3}\sin\left(hwt+\theta_h\right)}{2}+\frac{\cos\left(hwt+\theta_h\right)}{2}\right)=\\ &hw\left(A_h\cos\left(hwt+\theta_h\right)-B_h\cos\left(\frac{\pi}{3}-hwt-\theta_h\right)+C_h\cos\left(\frac{2\pi}{3}-hwt-\theta_h\right)\right)=hwi_{\alpha h}\end{aligned} \tag{14}$$

where A_h, B_h, and C_h are the amplitudes of the h^{th} harmonic current with positive, negative, and zero sequences, respectively.

B. Zero-sequence Harmonic Current

For the vector diagram presented in Fig. 3(b), the abc-$\alpha\beta$ transformation is performed on the h^{th} zero-sequence harmonic current to obtain (15) and (16).

$$i_{\alpha h}=3A_h\cos\left(hwt+\theta_h\right) \tag{15}$$

$$i_{\beta h}=3A_h\sin\left(hwt+\theta_h\right) \tag{16}$$

Then, derivatives of $i_{\alpha h}$ and $i_{\beta h}$ can be expressed as:

$$\frac{\mathrm{d}i_{\alpha h}}{\mathrm{d}t}=-3hwA_h\sin\left(hwt+\theta_h\right)=-hwi_{\beta h} \tag{17}$$

$$\frac{\mathrm{d}i_{\beta h}}{\mathrm{d}t}=3hwA_h\cos\left(hwt+\theta_h\right)=hwi_{\alpha h} \tag{18}$$

Based on the above analysis, (9) can be re-written as:

$$\begin{bmatrix}u_\alpha\\u_\beta\end{bmatrix}=\left(\sum_{h=1}^{H}\begin{bmatrix}i_{\alpha h} & -hi_{\beta h}\\ i_{\beta h} & hi_{\alpha h}\end{bmatrix}\right)\begin{bmatrix}R\\X\end{bmatrix} \tag{19}$$

$$X=wL \tag{20}$$

where X is the equivalent reactance at fundamental frequency. Sample point values of three-phase voltage and current are processed by the FFT, and the abc-$\alpha\beta$ transformation is performed on virtual waveforms of each harmonic current; then, equivalent impedance parameters are solved by (19). The solution to (19) is given by:

$$R=\frac{\left(\sum_{h=1}^{H}hi_{\alpha h}\right)u_\alpha+\left(\sum_{h=1}^{H}hi_{\beta h}\right)u_\beta}{\left(\sum_{h=1}^{H}i_{\alpha h}\right)\left(\sum_{h=1}^{H}hi_{\alpha h}\right)+\left(\sum_{h=1}^{H}i_{\beta h}\right)\left(\sum_{h=1}^{H}hi_{\beta h}\right)} \tag{21}$$

$$X=\frac{-\left(\sum_{h=1}^{H}i_{\beta h}\right)u_\alpha+\left(\sum_{h=1}^{H}i_{\alpha h}\right)u_\beta}{\left(\sum_{h=1}^{H}i_{\alpha h}\right)\left(\sum_{h=1}^{H}hi_{\alpha h}\right)+\left(\sum_{h=1}^{H}i_{\beta h}\right)\left(\sum_{h=1}^{H}hi_{\beta h}\right)} \tag{22}$$

In comparison to (3), the denominators of (21) and (22) are always greater than zero for three-phase symmetrical loads; thus, (19) avoids abnormal values caused by zero-crossing of the denominator.

However, the above-mentioned algorithm employs the FFT, which requires selecting the data cycle. For fewer cycles, the accuracy of the virtual waveform is limited. Conversely, if there are too many cycles, the tracking speed of the algorithm of the parameters' change will be decreased. Assuming that the abc-$\alpha\beta$ transformation is directly adopted to the three-phase voltage and current, the following expression can be obtained:

$$\begin{bmatrix}u_\alpha\\u_\beta\end{bmatrix}=\begin{bmatrix}i_\alpha & -i_\beta\\ i_\beta & i_\alpha\end{bmatrix}\begin{bmatrix}R\\X\end{bmatrix} \tag{23}$$

Compared with (19), the coefficient h of each harmonic current in (19) is ignored, so there are relative deviations of the elements in the first and second rows in the second column, which can be expressed as:

$$\varDelta_{12}=\frac{\sum_{h=2}^{H}(h-1)i_{\beta h}}{\sum_{h=1}^{H}hi_{\beta h}} \tag{24}$$

$$\varDelta_{22}=\frac{\sum_{h=2}^{H}(h-1)i_{\alpha h}}{\sum_{h=1}^{H}hi_{\alpha h}} \tag{25}$$

To avoid the FFT process and increase the parameter-change tracking speed of the algorithm, the above-given relative deviations are ignored, and a new equation based on the idea of regression is constructed as:

$$\begin{bmatrix} u_{1\alpha} \\ u_{1\beta} \\ u_{2\alpha} \\ u_{2\beta} \end{bmatrix} = \begin{bmatrix} i_{1\alpha} & -i_{1\beta} \\ i_{1\beta} & i_{1\alpha} \\ i_{2\alpha} & -i_{2\beta} \\ i_{2\beta} & i_{2\alpha} \end{bmatrix} \begin{bmatrix} R \\ X \end{bmatrix} \tag{26}$$

The solution to (26) is expressed by:

$$R = \frac{i_{1\alpha}u_{1\alpha} + i_{2\alpha}u_{2\alpha} + i_{1\beta}u_{1\beta} + i_{2\beta}u_{2\beta}}{i_{1\alpha}^2 + i_{2\alpha}^2 + i_{1\beta}^2 + i_{2\beta}^2} \tag{27}$$

$$X = \frac{i_{1\alpha}u_{1\beta} - i_{1\beta}u_{1\alpha} + i_{2\alpha}u_{2\beta} - i_{2\beta}u_{2\alpha}}{i_{1\alpha}^2 + i_{2\alpha}^2 + i_{1\beta}^2 + i_{2\beta}^2} \tag{28}$$

Equation (26) avoids abnormal values caused by the zero-crossing of the denominator.

Therefore, an innovative method for the calculation of equivalent impedance parameters of three-phase symmetrical loads is obtained, which is given by (19) and (26). In the following section, this method is applied to various practical cases to demonstrate its effectiveness and superiority.

IV. Case Study

A. Cases with an Equivalent Circuit of a Load in Time Domain

Based on the equivalent series impedance model shown in Fig. 1, a three-phase symmetrical simulation model has been constructed on MATLAB/Simulink platform to acquire sample point values of three-phase voltage and current, where the phase voltage is 220 V, and the frequency is 50 Hz. The sampling frequency of simulation data is 12.8 kHz, which is consistent with the sampling frequency of most power quality monitoring devices. To validate the proposed method, four different cases are analyzed, which are described as follows.

1) The resistance is 10 Ω, and the inductance is 0.01 H, which represent a linear load.

2) The resistance is a 200 Hz sine wave with amplitude between 10-20 Ω, and the inductance is always 0.015 H.

3) The resistance is 10 Ω, and the inductance is a 200 Hz sine wave with amplitude between 0.01-0.02 H.

4) The resistance is a 100 Hz triangular wave with an amplitude between 10-20 Ω, and the inductance is a 200 Hz sine wave with amplitude between 0.01 H and 0.02 H.

The first case is configured to examine the precision under the assumption of constant equivalent impedance; the second and third cases are designed to examine the precision of solution when one of the resistance and inductance is constant while the other varies with time; the fourth case is used to evaluate the solving precision when the resistance and inductance are both time-varying.

Equations (2), (19), and (26) are used to solve the equivalent impedance parameters for the above-mentioned four cases. Equation (2) defines a traditional method labeled as Method I in this paper; and (19) and (26) define Methods II and III, respectively. The calculated resistance and inductance waveforms at the maximum frequency of 2550 Hz in FFT analysis are shown in Fig. 4. Furthermore, the mean value (μ) and standard deviation (σ) of the relative error of all methods are calculated, as shown in Table I, and a histogram shown in Fig. 5 is provided to achieve a more intuitive comparison of the results.

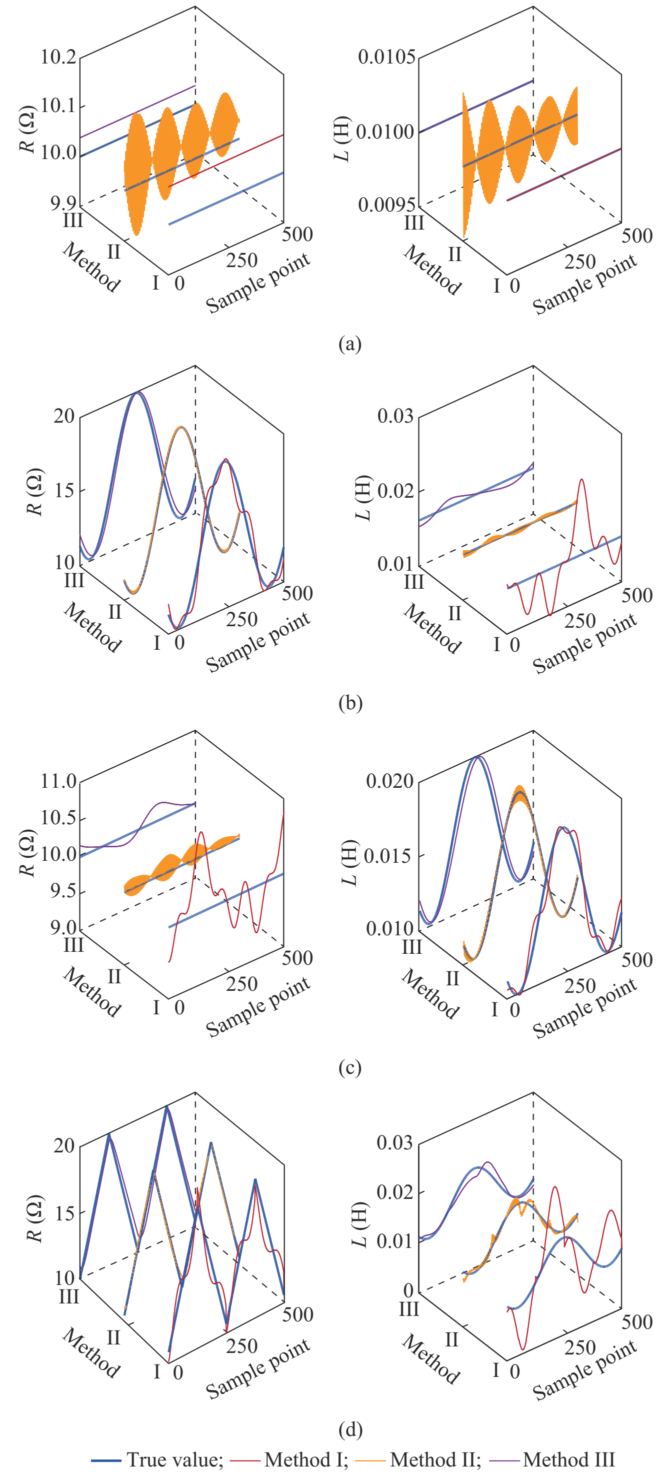

Fig. 4. Calculated resistance and inductance waveforms at the maximum frequency of 2550 Hz in FFT analysis. (a) Case 1. (b) Case 2. (c) Case 3. (d) Case 4.

Except for Case 1, the accuracy of Methods II and III is much better than that of Method I. Furthermore, the accuracy of Method III is slightly lower than that of Method II since it ignores the deviation of (24) and (25). In addition, compared with the proposed method, the equivalent impedance waveforms of nonlinear load obtained by Method I deviate significantly from the real waveforms.

TABLE I
MEAN AND STANDARD DEVIATIONS OF RELATIVE ERROR OF EACH METHOD

Case	Parameter	Relative error (%)					
		Method I		Method II		Method III	
		μ	σ	μ	σ	μ	σ
1	R	0.7710	9×10^{-10}	0.5013	0.3743	0.3855	1×10^{-8}
	L	2×10^{-10}	6×10^{-10}	1.2257	0.9834	0.0100	6×10^{-9}
2	R	4.0816	3.8469	0.6377	0.4779	3.8469	1.2965
	L	19.2825	19.6920	1.2965	0.9571	3.8522	2.0427
3	R	3.2563	2.8659	0.6877	0.5271	0.9411	0.6539
	L	4.3843	3.4761	1.2267	0.9718	4.3401	2.2373
4	R	7.0512	4.0217	1.4753	1.3489	4.7448	2.3646
	L	39.1099	31.9961	4.2474	3.2070	6.2682	3.8958

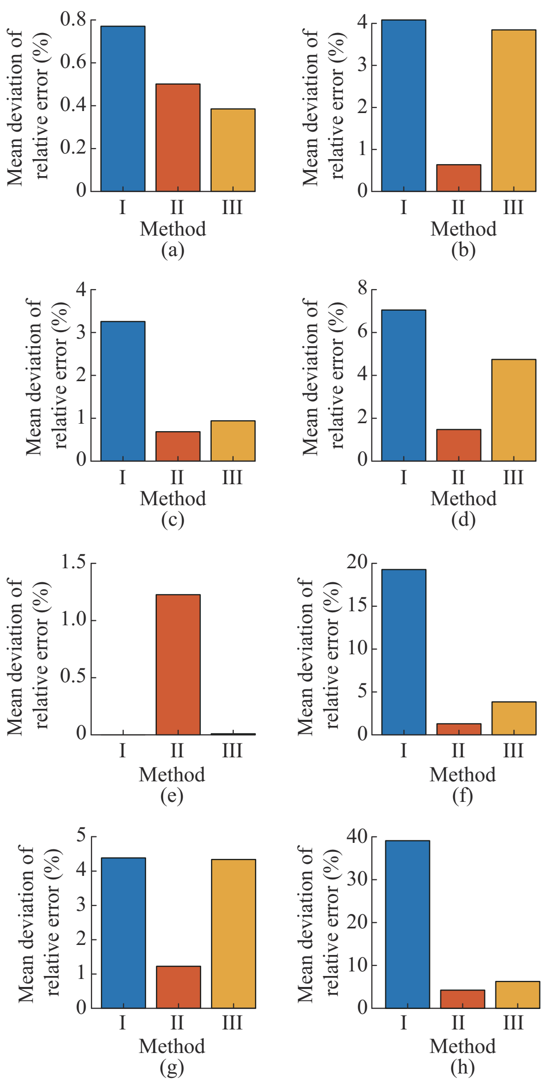

Fig. 5. Mean deviation of relative error of calculated impedance parameters. (a) Resistance for Case 1. (b) Resistance for Case 2. (c) Resistance for Case 3. (d) Resistance for Case 4. (e) Inductance for Case 1. (f) Inductance for Case 2. (g) Inductance for Case 3. (h) Inductance for Case 4.

Since the equivalent impedance is constant in Case 1, which does not meet the generation of zero-crossing of the denominator [21], Method I is not affected, and Method III does not have the deviation, indicating that the accuracy of these methods is high. However, Method II requires the FFT analysis and thus is influenced by the accuracy of FFT. The superposition of the virtual harmonic current waveforms could not completely reproduce the original waveform; thus, the relative error of Method II is larger than that of Methods I and III. The deviation between the superposition of the virtual harmonic current waveforms and the original waveform is shown in Fig. 6.

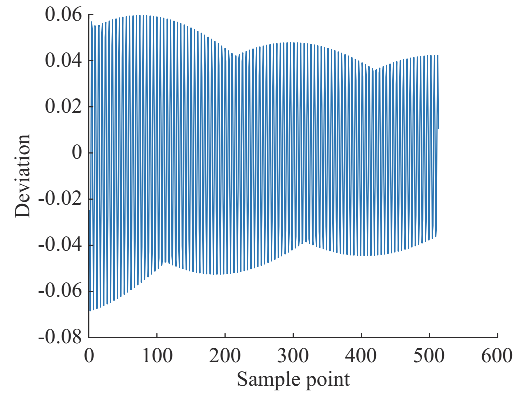

Fig. 6. Deviation between superposition of virtual harmonic current waveform and original waveform.

As shown in Fig. 4, the equivalent impedance waveforms calculated by Method II have a small amplitude high-frequency oscillation. In Case 1, the equivalent impedance waveforms obtained by Method II are subjected to the Hilbert Huang transform (HHT) to obtain the Hilbert spectrum, as shown in Fig. 7. The high-frequency component is around 2500 Hz, which is close to the specified maximum frequency of 2550 Hz used in the FFT analysis. It should be noted that the Hilbert spectra of the equivalent impedance waveforms obtained by Method II in the other cases also have high-frequency components near 2500 Hz, but these are not shown here due to space constraints.

If the maximum frequency for the FFT analysis is 5050 Hz, and the maximum harmonic order considered is 100, the Hilbert spectrum of equivalent impedance waveforms solved by Method II for Case 1 is shown in Fig. 8.

As illustrated in Figs. 7 and 8, the high-frequency component in the equivalent impedance waveforms calculated by Method II is closely related to the specified maximum frequency in the FFT analysis. Therefore, an appropriate low-pass filter could be used to remove the high-frequency component, providing smoother equivalent impedance waveforms. Therefore, the low-pass function provided by MATLAB software is used in this paper, and its parameters are all set to default values except for the passband frequency. Namely, the passband frequency is set to be 4550 Hz, which is lower than the maximum frequency in the FFT of 5050 Hz but significantly higher than the impedance signal fluctuation frequency. The resistance and inductance waveforms solved by Method II before and after filtering are shown in Fig. 9.

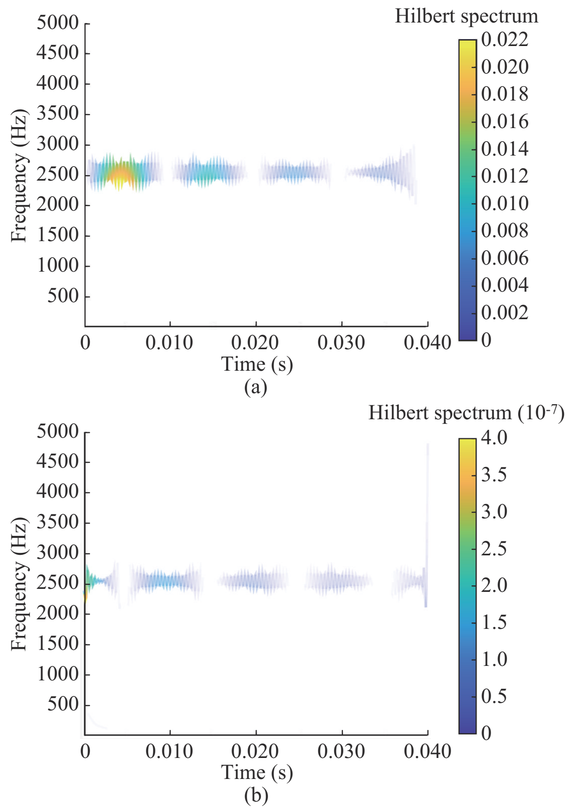

Fig. 7. Hilbert spectrum of equivalent impedance waveforms obtained by Method II for Case 1 when the maximum frequency in FFT analysis is 2550 Hz. (a) Hilbert spectrum of equivalent resistance waveform. (b) Hilbert spectrum of equivalent inductance waveform.

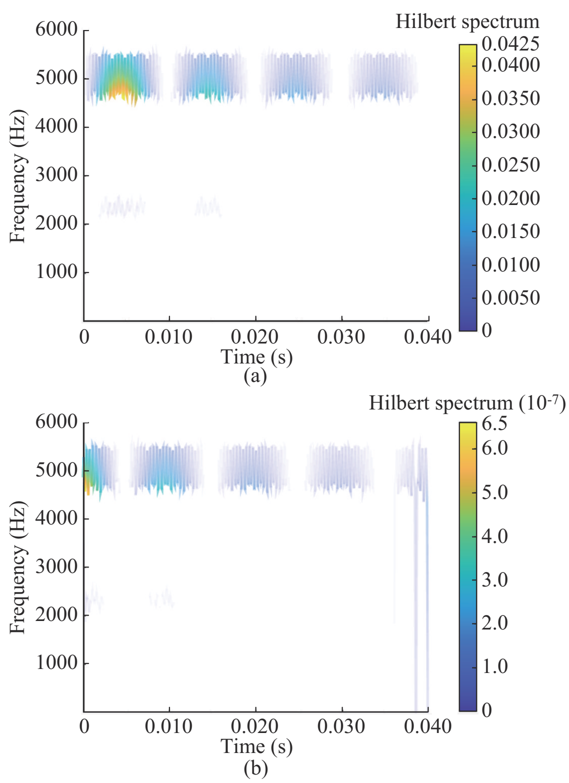

Fig. 8. Hilbert spectrum of equivalent impedance waveforms obtained by Method II for Case 1 when the maximum frequency for FFT analysis is 5050 Hz. (a) Hilbert spectrum of equivalent resistance waveform. (b) Hilbert spectrum of equivalent inductance waveform.

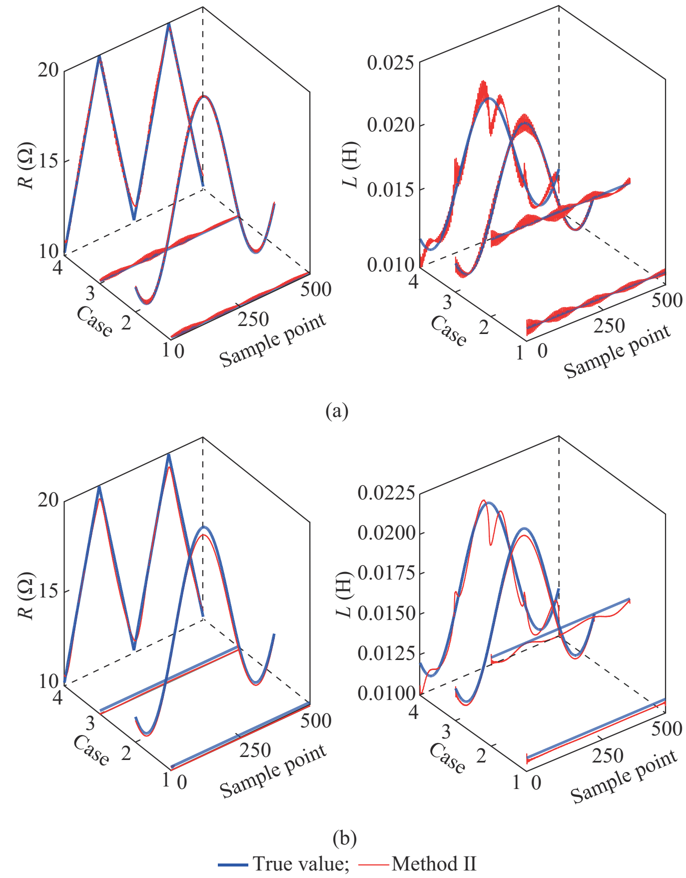

Fig. 9. Resistance and inductance waveforms solved by Method II before and after filtering. (a) Before filtering. (b) After filtering.

The strengths, weaknesses, and application scenarios of the three methods are obtained based on the results of the case in this subsection, and are shown in Table II.

TABLE II
STRENGTHS, WEAKNESSES, AND APPLICATION SCENARIOS OF THREE METHODS

Method	Strength	Weakness	Application scenarios
Method I	Easy to implement	Prone to outliers	Single and three-phase loads under non-zero-crossing conditions
Method II	Avoiding outliers; high accuracy for nonlinear loads	Requiring more than adjacent sample point values	Three-phase symmetrical loads
Method III	Avoiding outliers; high tracking speed of parameters' change	Less accurate for nonlinear loads	Three-phase symmetrical loads

B. Cases with Simulink Simulation of Comprehensive Loads

Modern nonlinear loads can be roughly classified into three types based on the harmonic current generation mechanism type, i. e., ferromagnetic saturation, electric arc, and power electronics, and their representatives are denoted by transformers, electric arc furnaces (EAFs), and rectifiers, respectively.

The Simulink simulation scheme of three-phase comprehensive loads is shown in Fig. 10. This scheme is constructed to verify the effectiveness of the proposed method of equivalent impedance parameter calculation used for harmonic source location.

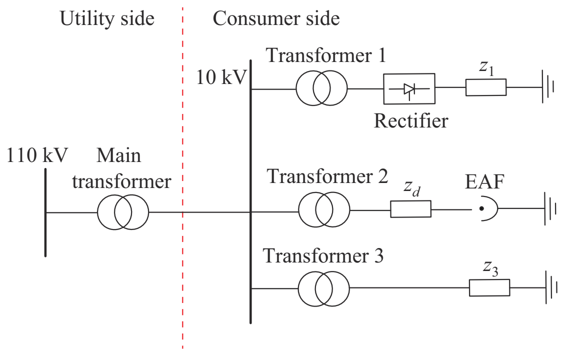

Fig. 10. Simulink simulation of three-phase comprehensive loads.

In Fig. 10, z_1 is the equivalent impedance of the rectifier on the DC side; z_3 is a linear load; and z_d is the equivalent impedance, which groups the lead and electrode of the EAF. The EAF model is designed according to the procedure given in [25], and the simulation parameters are set as shown in Table III.

TABLE III
SIMULATION PARAMETERS

Load	Parameter	Value
Linear load	Resistance (Ω)	120
	Inductance (H)	0.1
EAF	Equivalent resistance (μΩ)	419.9
	Equivalent inductance (μH)	9.55
	Capacity (MVA)	40
Rectifier	Number of pulses	12
	Resistance (Ω)	250
	Inductance (H)	0.5

The equivalent impedance waveforms of comprehensive loads obtained by the three methods are shown in Fig. 11, where a large number of outliers in the waveforms obtained by Method I can be observed. The waveforms calculated by Methods II and III have similar shapes but different amplitudes. Namely, the amplitudes of the waveforms calculated by Method III are smaller than those solved by Method II.

The results of the NLI and total harmonic current distortion THD_i are shown in Table IV, where it can be observed that the difference in the NLI between the linear and nonlinear loads obtained by Methods II and III is about 60 times more than that by Method I, which is helpful to locate the harmonic source. In addition, the NLI results of Methods II and III follow the same trend as the THD_i, whereas the NLI result of Method I deviates from the THD_i trend. Specifically, based on Method I, the NLI value of the EFA method is larger than that of the rectifier.

Based on Fig. 11, there are a large number of outliers in the waveforms of the equivalent impedance obtained by Method I, which affects the calculation result of NLI, reduces the difference in the NLI value between linear and nonlinear loads, and could cause misjudgment or failure of the harmonic source location.

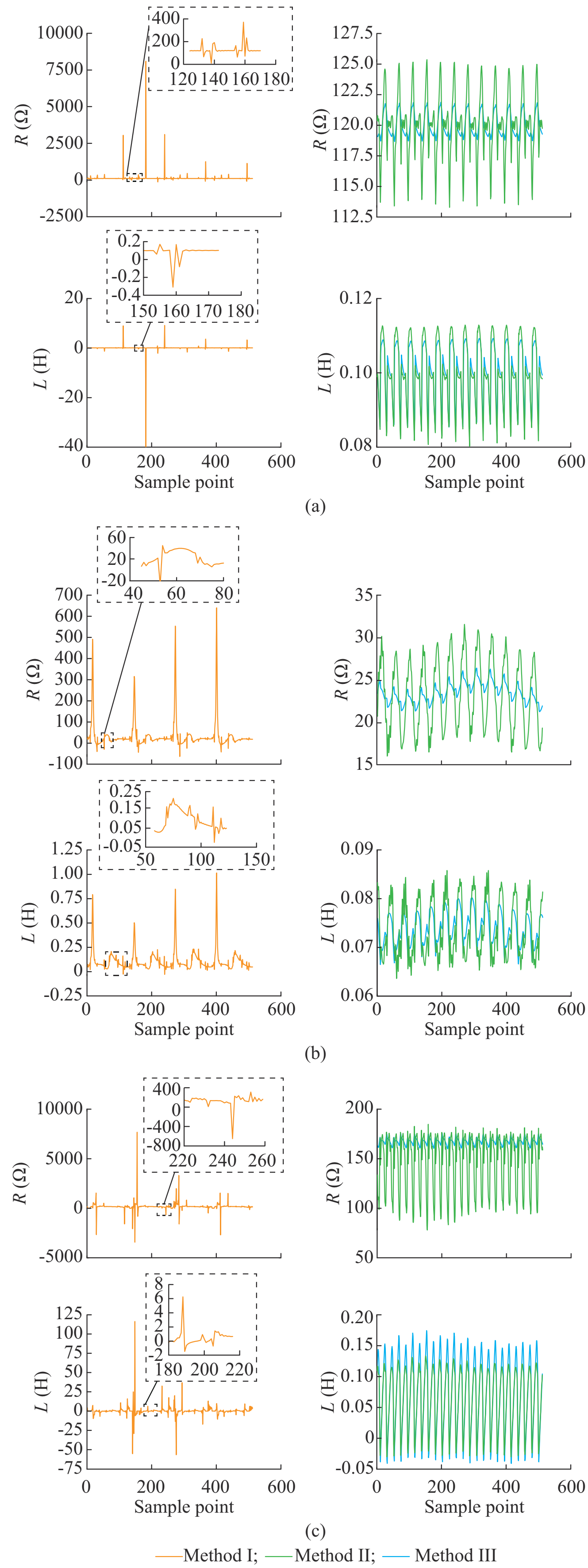

Fig. 11. Equivalent impedance waveforms of comprehensive loads obtained by different methods. (a) Linear load. (b) EAF. (c) Rectifier.

TABLE IV
NLI AND THD_i OF LOADS

Load	NLI			THD_i (%)
	Method I	Method II	Method III	
Linear load	0.2105	0.0055	0.0056	0.97
EAF	1.5407	0.3478	0.3165	9.30
Rectifier	0.9220	0.3575	0.3892	11.02

C. Cases with Actual Monitoring Data of EAF

In this test, a 55 t EAF in a steelmaking plant is used as an example. The power supply diagram is shown in Fig. 12; the potential transformer (PT) and the current transformer (CT) are used to monitor the voltage of the 35 kV bus and EAF current, respectively. In Fig. 12, T1 denotes the main transformer of the steelmaking plant, and T2 is the EAF transformer (type HSSPZ-38000/35). The static var compensator (SVC) is used to govern voltage fluctuation and flicker.

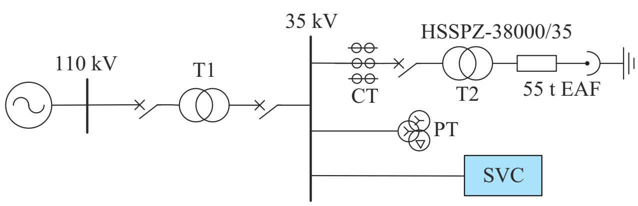

Fig. 12. Power supply diagram of 55 t EAF.

The measured three-phase voltage and current waveforms of the EAF whose transformer's rated capacity is 38 MVA are shown in Fig. 13.

Based on the measured data, the equivalent impedance waveforms are obtained, as shown in Fig. 14. As shown in Fig. 14, the resistance waveform of Method I is filled with mass of spikes, although it could barely show the characteristics. The inductance waveform obtained by Method I is like noise. However, the equivalent impedance waveforms of Methods II and III are smooth and similar to the simulation results of the EAF in Fig. 11(b). In addition, the NLI and THD_i of the EAF's measured data are shown in Table V.

Based on the results in Table V, the NLI based on Method I is larger than that based on Methods II and III, which is consistent with simulation results in the case of this subsection.

The above analysis demonstrates the applicability of the proposed method in practical engineering.

V. CONCLUSION

In this paper, an efficient method of equivalent impedance parameter calculation of three-phase symmetrical loads for harmonic source location is proposed. Combined with the FFT and abc-$\alpha\beta$ transformation, a set of equations based on the relationship between current and voltage of the equivalent circuit are constructed to solve equivalent impedance waveforms, which generally avoids outliers caused by the zero-crossing of the denominator. The results obtained under three cases are discussed, and the corresponding conclusions can be summarized as follows.

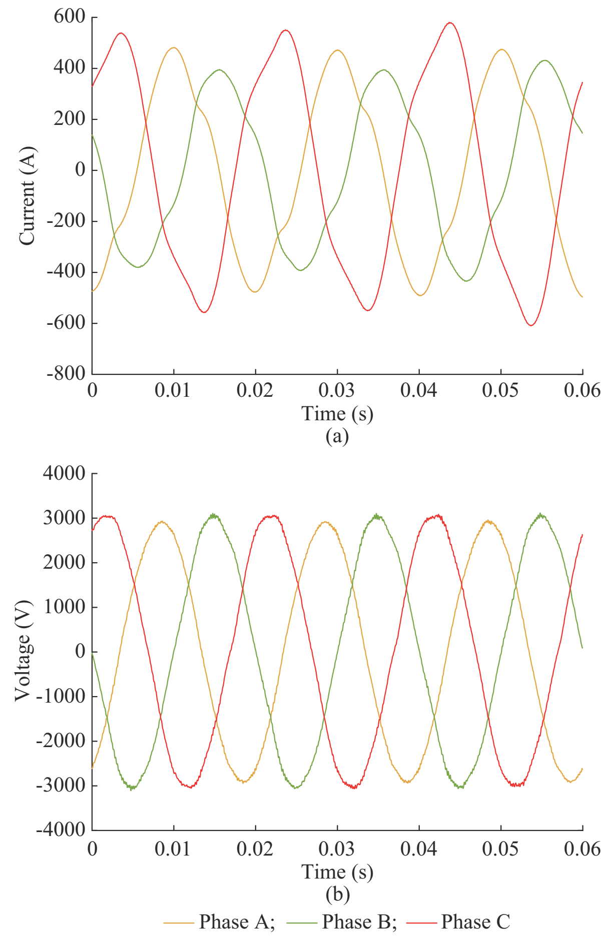

Fig. 13. Measured three-phase voltage and current waveforms obtained by EAF. (a) Current waveforms. (b) Voltage waveforms.

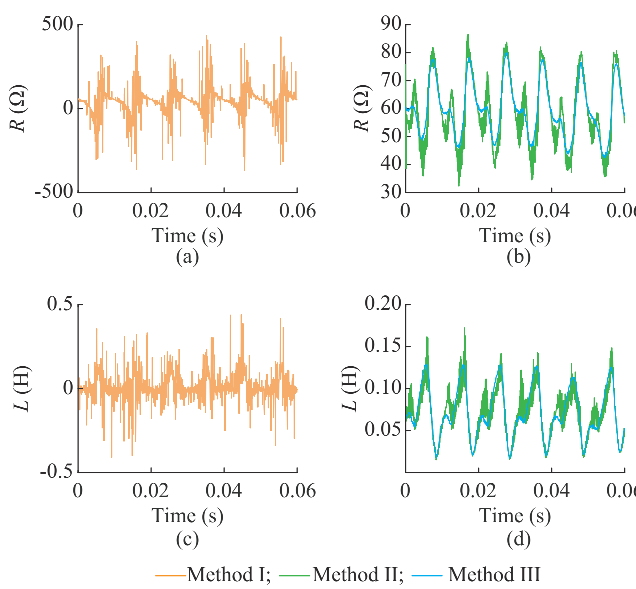

Fig. 14. Equivalent impedance waveforms of EAF's measured data.

TABLE V
NLI AND THD_i OF EAF'S MEASURED DATA

NLI			THD_i (%)
Method I	Method II	Method III	
0.4177	0.1649	0.1656	4.80

1) Compared with the traditional equivalent impedance parameter calculation method, the proposed method is not only simpler, easier to implement, and more accurate, but also able to avoid outliers.

2) The results show that the waveforms solved by one of the calculation equations proposed in this paper contain a small-amplitude high-frequency oscillation, whose frequency is closely related to the specified maximum frequency in the FFT analysis. Therefore, these components can be filtered using an appropriate low-pass filter.

3) According to equivalent impedance waveforms solved using the proposed method, the difference in the NLI between the linear and the nonlinear loads is significant, which is helpful in harmonic source localization.

REFERENCES

[1] F. M. Camilo, M. E. Almeida, R. Castro *et al.*, "Multi-conductor line models for harmonic load-flow calculations in LV networks with high penetration of PV generation," *Journal of Modern Power Systems and Clean Energy*, vol. 10, no. 5, pp. 1288-1301, Sept. 2022.

[2] Y. Pu, Q. Shu, and F. Xu, "Harmonic amplification analysis of cable lines with distributed parameters based on Kalman filter and convolution inversion," *Journal of Modern Power Systems and Clean Energy*, vol. 11, no. 6, pp. 1804-1813, Nov. 2023.

[3] *IEEE Recommended Practice and Requirements for Harmonic Control in Electric Power Systems*, IEEE Standard 519-2014, 2014.

[4] M. Dalali and A. Jalilian, "Indices for measurement of harmonic distortion in power systems according to IEC 61000-4-7 standard," *IET Generation Transmission & Distribution*, vol. 9, no. 14, pp. 1903-1912, Nov. 2015.

[5] F. Xu, C. Wang, K. Guo *et al.*, "Harmonic sources' location and emission estimation in underdetermined measurement system," *IEEE Transactions on Instrumentation and Measurement*, vol. 70, pp. 1-11, May 2021.

[6] K. Tang and C. Shen, "Harmonic emission level assessment method based on parameter identification analysis," *IET Generation Transmission & Distribution*, vol. 13, no. 7, pp. 976-983, Apr. 2019.

[7] L. Cristaldi and A. Ferrero, "Harmonic power flow analysis for the measurement of the electric power quality," *IEEE Transactions on Instrumentation and Measurement*, vol. 44, no. 3, pp. 683-685, Jun. 1995.

[8] W. Xu and Y. Liu, "A method for determining customer and utility harmonic contributions at the point of common coupling," *IEEE Transactions on Power Delivery*, vol. 15, no. 2, pp. 804-811, Apr. 2000.

[9] R. Azouaou, S. Rabahallah, and S. Leulmi, "Study of the direction of the harmonic injections in the electrical power systems," in *Proceedings of 39th International Universities Power Engineering Conference*, Bristol, England, Sept. 2004, pp. 944-947.

[10] C. Li, W. Xu, and T. Tayjasanant, "A 'critical impedance'-based method for identifying harmonic sources," *IEEE Transactions on Power Delivery*, vol. 19, no. 2, pp. 671-678, Apr. 2004.

[11] W. Xu, X. Liu, and Y. Liu, "An investigation on the validity of power-direction method for harmonic source determination," *IEEE Transactions on Power Delivery*, vol. 18, no. 1, pp. 214-219, Jan. 2003.

[12] B. Wang, G. Ma, J. Xiong *et al.*, "Several sufficient conditions for harmonic source identification in power systems," *IEEE Transactions on Power Delivery*, vol. 33, no. 6, pp. 3105-3113, Dec. 2018.

[13] X. Xiao, R. Zhou, X. Ma *et al.*, "A novel method for estimating utility harmonic impedance based probabilistic evaluation," *IET Generation, Transmission & Distribution*, vol. 16, no. 7, pp. 1438-1448, Jan. 2022.

[14] G. T. Heydt, "Identification of harmonic sources by a state estimation technique," *IEEE Transactions on Power Delivery*, vol. 4, no. 1, pp. 569-576, Jan. 1989.

[15] N. Kanao, M. Yamashita, H. Yanagida *et al.*, "Power system harmonic analysis using state-estimation method for Japanese field data," *IEEE Transactions on Power Delivery*, vol. 20, no. 2, pp. 970-977, Apr. 2005.

[16] E. Sezgin, M. Göl, and Ö. Salor, "State-estimation-based determination of harmonic current contributions of iron and steel plants supplied from PCC," *IEEE Transactions on Industry Applications*, vol. 52, no. 3, pp. 2654-2663, May-Jun. 2016.

[17] Y. Wang, R. Xu, X. Ma *et al.*, "Harmonic state estimation based on graph signal processing," *IET Generation, Transmission & Distribution*, vol. 16, no. 6, pp. 1083-1095, Jan. 2022.

[18] M. M. M. E. Arini, "A time domain load modelling technique and harmonics analysis," in *Proceedings of 8th International Conference on Harmonics and Quality of Power*, Athens, Greece, Oct. 1998, pp. 930-938.

[19] A. A. Moustafa, A. M. Moussa, and M. A. El-Gammal, "Separation of customer and supply harmonics in electrical power distribution systems," in *Proceedings of 9th International Conference on Harmonics and Quality of Power*, Orlando, USA, Oct. 2000, pp. 1035-1040.

[20] Y. Liu, H. Gong, X. Xiao *et al.*, "Harmonic source location at the point of common coupling based on the nonlinearity index of load," in *Proceedings of 2009 Asia-Pacific Power and Energy Engineering Conference*, Wuhan, China, Mar. 2009, pp. 1-5.

[21] K. Tang, C. Shen, S. Liang *et al.*, "Outlier issues in harmonic source location based on parameter identification method," in *Proceedings of 2016 IEEE PES General Meeting*, Boston, USA, Jul. 2016, pp. 1-5.

[22] Y. Zhang, C. Lin, Z. Shao *et al.*, "A non-intrusive identification method of harmonic source loads for industrial users," *IEEE Transactions on Power Delivery*, vol. 37, no. 5, pp. 4358-4369, Oct. 2022.

[23] E. Thunberg and L. Soder, "A Norton approach to distribution network modeling for harmonic studies," *IEEE Transactions on Power Delivery*, vol. 14, no. 1, pp. 272-277, Jan. 1999.

[24] X. Xiao, *Analysis and Control of Power Quality*. Beijing: China Electric Power Press, 2010, pp. 161-162.

[25] F. Lin, Y. Lin, D. Huang *et al.*, "Ultra-high-power arc furnace model for low frequency non-stationary inter-harmonics," in *Proceedings of 2020 5th Asia Conference on Power and Electrical Engineering*, Chengdu, China, Jun. 2020, pp. 2049-2053.

Yi Zhang received the B.S. and Ph.D. degrees in power system and automation from Sichuan University, Chengdu, China, in 2007 and 2012, respectively. From 2012 to 2014, he was a Postdoctoral Fellow with Zhejiang University, Hangzhou, China. From 2015 to 2017, he was a Senior Engineer with State Grid Power Quality Analysis Lab, State Grid Fujian Electric Power Research Institute, Fuzhou, China. Since 2018, he has been Associate Professor with Fuzhou University, Fuzhou, China. His research interests include power quality data analysis, voltage sag analysis and management, and active distribution system.

Bijie Liu received the B.S. degree in power system and automation from Fuzhou University, Fuzhou, China, in 2020. He is currently pursuing the M.S. degree in electrical engineering in Fuzhou University, Fuzhou, China. His research interests include power system harmonic analysis and evaluation.

Caihua Lin received the B.S. and M.S. degrees in power system and automation from Fuzhou University, Fuzhou, China, in 2019 and 2022, respectively. He is currently working as a Researcher in State Grid Fujian Electric Power Research Institute, Fuzhou, China. His research interests include power system harmonic analysis and evaluation, and relay protection of power system.

Zhenguo Shao received the B.S., M.S., and Ph.D. degrees in electrical engineering from Southeast University, Nanjing, China, in 1992, 2001, and 2004, respectively. From 1992 to 1995, he was an Electrical Engineer with Nantong Hong Yang Industrial Company Ltd., Nantong, China. From 1995 to 1998, he was a Lecturer with Nantong University, Nantong, China. From 2004 to 2006, he was a Postdoctoral Researcher with the Fujian Electric Power Company, Fuzhou, China. Since 2006, he has been with the College of Electrical Engineering and Automation, Fuzhou University, Fuzhou, China, where he is currently a Full Professor and an Associate Dean. He is also the Director of the Fujian Smart Electrical Engineering Technology Research Center. His main research interests include power quality monitoring and mitigation, smart grid control and operation, smart energy utilization, and big data analysis for smart grid.

Yuncong Xu received the B. S. degree in power system and automation from Jishou University, Jishou, China, in 2021. He is currently pursuing the M.S. degree in power system and automation in Fuzhou University, Fuzhou, China. His research interests include power system harmonic analysis and evaluation, and electric arc furnace.